Electronic Supplementary Information

Robust Hydrogels with Hierarchical Porosities from the Controlled Assembly of Metal-Organic Polyhedra for Rapid Removal of Low-Concentration Aqueous Iodine

Haiyan Xiao,[‡a] Jia-Fu Yin,[‡a] Hanqiu Jiang, [b] Linjie Lan, [a] Jiadong Chen, [a] Wei Liu-Fu, [a] Shengqiu Liu, [a] Yubin Ke, [b] and Panchao Yin*[a]

[‡] These authors contribute equally to this work.

[a] State Key Laboratory of Luminescent Materials and Devices & South China Advanced Institute for Soft Matter Science and Technology, Guangdong Basic Research Center of Excellence for Energy & Information Polymer Materials, South China University of Technology, Guangzhou 510640, P. R. China

[b] China Spallation Neutron Source, Institute of High Energy Physics, Chinese Academy of Science, Dongguan, 523000, P. R. China

*Corresponding author. E-mail: yinpc@scut.edu.cn

Table of contents:

1. Materials and Solvents

Materials: *p* - Toluenesulfonyl chloride (TsCl) (99 %, Aladdin), triethylamine (TEA) (99.0 %, Aladdin), imidazole (99 %, Aladdin), sodium hydride (NaH) (60 %, Aladdin), sodium hydroxide (NaOH) (≥ 98 %, Aladdin), poly(ethylene glycol) (average *M*w = 400) (98 %, TCI Reagent), poly(ethylene glycol) (average *M*w = 2k) (98 %, Adamas), isonicotinoyl chloride hydrochloride (95 %, Energy Chemical), poly(ethylene glycol) diacrylate (average *M*w =1k) ($PEGDA_{1k}$) (98 %, Aladdin), iodine (≥ 99.8 %, Aladdin), six-arms poly(ethylene glycol) (average *M*w = 2k) (6 arms-PEG_{2k}) (95 %, Liming Research & Design Institute of Chemical Industry), four-arms poly(ethylene glycol) imidazole (average *M*w = 2k) (4 arms-PEG_{2k}-CDI) (98 %, ShangHai ToYongBio Tech.Inc), carbonyl-imidazole-poly(ethylene glycol)-carbonyl-imidazole (average *M*w = 3.4k) ($PEG_{3.4k}$-CDI_2) (98 %, Aladdin), sodium sulfate anhydrous (99 %, Aladdin).

Solvents: Methanol (99.5 %, Aladdin), tetrahydrofuran (THF) (≥ 99.8 %, General-reagent), dichloromethane (DCM) (≥ 99.5 %, General-reagent), acetonitrile (≥ 99.5 %, General-reagent), chloroform-*d* (99.8 %, Aladdin), all organic solvents or monomers were used without further purification. Deionized water was obtained from the Ultra-pure water system (Water Purifier, WP-RO-10B).

2. Methods

2.1 Nuclear Magnetic Resonance (NMR) Spectroscopy.

All the samples were dissolved in deuterium solvents with tetramethylsilane (TMS) as reference. ^{1}H NMR has recorded on Bruker AVANCE II 500 spectrometer at 298 K.

2.2 Isothermal Titration Calorimetry (ITC).[1]

The isothermal titration experimental data of telechelic ligands with MOP were measured by an isothermal titration calorimeter (Malvern, MicroCal PEAQ-ITC). In the ITC assay (RT), the MOP aqueous solution was placed in a temperature-controlled sample cell, and coupled with a reference cell filled with H_2O through a thermocouple

loop, the sample cell (MOP aqueous solution) and the reference cell (H_2O) in the same external environment. The telechelic ligands aqueous solution (30 μL) was added dropwise into the MOP aqueous solution through an isothermal titration calorimeter. When the MOP aqueous solution reacted with the telechelic ligands aqueous solution, the temperature of the sample cell and the reference cell would change accordingly. The instrument can detect the energy change during the titration process, and the thermodynamic parameters of the titration process can be obtained by further fitting the experimental data with the processing software that comes with the instrument.

2.3 Scanning Electron Microscope (SEM).

JEOL JSM-7900F SEM was exploited to characterize the microstructures of the MOP hydrogels. The afforded hydrogels were fixed on the SEM sample table and then frozen in a liquid nitrogen chamber during vacuolization, then transferred to the sample chamber. After sublimating for 15 minutes to remove the solvents, the hydrogels were sprayed with gold (5 mA, 45 s) to improve the conductivity. After that, these samples are used for further cryo-SEM experiments at 5 kV.

The MOP hydrogels were freeze-dried and spread on a sample stand with conductive tape. The samples were sprayed with gold (30 mA, 45 s) before imaging to improve the conductivity for further SEM experiments at 5 kV and energy dispersive X-ray analysis (EDX) at 15 kV.

2.4 Transmission Electron Microscopy (TEM).

The MOP hydrogels were freeze-dried and dispersed in ethanol at a concentration of 2.0 mg mL^{-1}. Then a small amount of the suspension liquids dropped onto a holey carbon film placed on a copper grid was dried and used to take images with a digital CCD camera in a JEOL-1230 microscope with an accelerating voltage of 120 keV.

2.5 Small Angle X-ray Scattering (SAXS).

The MOP hydrogels were sealed in a custom-made hollow U-shaped sample container with two layers of 3M tape. The MOP aerogels were sealed by two layers of 3M tape. The SAXS data were recorded on the beamline (BL-16B) of the Shanghai Synchrotron Radiation Facility (SSRF) with a Pilatus 2M detector. The wavelength of the incident X-ray beam is 1.23984 Å and the exposure time was set to 20 s to collect the structural

information. Silver behenate (AgBh) was used as the standard sample for calibration. For all the samples, the background was the two layers of 3M tape. Fit2D software is used to convert two-dimensional scattering data into a one-dimensional scattering curve. In contrast, while the contribution of background scattering is subtracted, and the real one-dimensional scattering data is finally obtained.

2.6 Small angle neutron scattering (SANS).

SANS data were collected at China Spallation Neutron Source (CSNS). Rh-MOP was dispersed in deuterium oxide (D_2O) to improve the contrast and the volume ratio was around 2%. The wavelength of the incident neutron was 1.2 ~ 9.5 Å and the exposure time for each sample was 2 h to acquire the form factor of Rh-MOP. For the MOP hydrogels, the hydrogels were formed in situ within D_2O in a quartz container with a thickness of 1 mm. The MOP hydrogels were exposed to the neutron beams and the scattered neutrons were detected by the area detector. The obtained two-dimensional data were then converted to one-dimensional data. The solvent background was subtracted to afford the final scattering curve.

2.7 Rheology.

A controlled-stress rotational rheometer (Anton Paar MCR-302) with parallel plate geometry was used to investigate the rheological properties of MOP hydrogels. Amplitude sweeps with constant frequency (ω = 5 rad s^{-1}) at 25 °C were performed to determine the linear viscoelastic region. Bearing this in mind, small amplitude oscillatory shear (SAOS) experiments were subsequently carried out to quantitatively evaluate the viscoelastic performances of different MOP hydrogels within the frequency window ranging from 0.1 ~ 100 rad s^{-1} at 25 °C. To ensure the credibility of the experiment data, the rheology experiments for each sample were repeated at least 2 times. The storage modulus (G') and loss modulus (G'') were obtained from the above-mentioned dynamic rheology experiments.

2.8 Diffusion spectrometer (DWS).

The DWS experiment was performed on a DWS RheoLab III (RHL-0019-0095) to obtain the intensity correlation functions of samples. Each sample was loaded into a quartz container with a thickness of 2 mm. During the experiment, the temperature was

controlled and maintained at T = 60 ± 0.1 °C. The scattered light of the gelation process was collected in a transmission or backscattering geometry to obtain normalized intensity autocorrelation function $g_2(\tau)$-1.

2.9 UV-Vis Spectroscopy.

MOP-based hydrogels (100 μL), $PEGDA_{1k}$ hydrogels (100 μL) and Rh-MOP were immersed in iodine aqueous solution (1 mM, 2 mL) at RT. The UV-Vis absorption spectra were measured at certain time intervals in a range of 200 ~ 800 nm on a Shimadzu UV-1800 spectrophotometer.

2.10 Scattering data analysis.[2,3]

The intensity of scattered radiation as a function of the scattering wavevector Q defined as:

$$Q = \frac{4\pi}{\lambda} sin(\frac{\theta}{2})$$

where λ is the wavelength of incident radiation and θ is the angle between the incident radiation and the detector measuring the scattered intensity.

The Sasview software was used to fit scattering data. The CRYSOL program was used to calculate the theoretical SAXS curve of Rh-MOP.

An empirical functional form (correlation length model) for scattering data characterized by low Q signal and high Q signal. The fitting model is expressed as below:

$$I(Q) = \frac{\alpha}{Q^n} + \frac{\beta}{(Q\xi)^m} + I_{\text{background}}$$

The first term describes Porod scattering from network inhomogeneities (exponent = n) and the second term is a Lorentzian function describing scattering from mesh-size structures of polymer chains (exponent = m). α and β are constants of proportionality indicative of the relative contrast and concentration, $I_{\text{background}}$ is the Q-invariant incoherent background. The parameter ξ is a correlation length for the experiments system.

3. Experimental Section

3.1 Synthesis of telechelic ligands

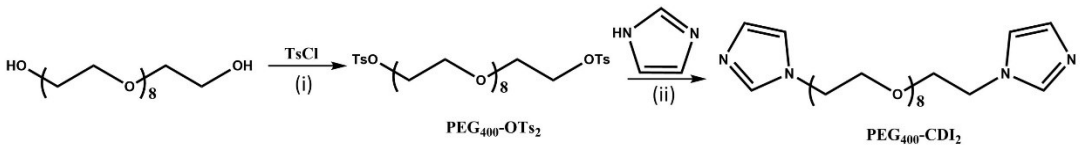

Scheme S1. Reaction conditions: (i) TsCl, TEA, DCM, 0 °C; (ii) imidazole, NaH, THF, 60 °C.

Synthesis of PEG_{400}-OTs_2: PEG_{400} (5.0 g, 12.5 mmol) and TEA (5.06 g, 50.0 mmol) were dissolved in DCM (50 mL), and then cooled down to 0 °C in an ice bath. TsCl (4.77 g, 25.0 mmol) was dissolved in DCM (25 mL) and added dropwise into the mixture under rapid stirring. The solution was stirred at 0 ~ 5 °C for 4 h and at room temperature for 20 h. The resulting solid was washed with deionized water, dried with anhydrous Na_2SO_4, and the crude residue was purified by flash chromatography (DCM:CH_3OH, 19:1), then filtered and dried in *vacuo*. Yield: 4.0 g, 45%. ^1H NMR (500 MHz, $CDCl_3$): δ 7.78 (d, 2H), 7.34 (d, 4H), 4.14 (t, 4H), 3.67 (t, 4H), 3.64 - 3.59 (m, 28H), 2.44 (s, 6H).

Synthesis of PEG_{400}-CDI_2: NaH (0.36 g, 15.0 mmol) and imidazole (0.68 g, 10.0 mmol) were dispersed in THF (20 mL) at RT until the solution became homogeneous. PEG_{400}-OTs_2 (2.0 g, 5.0 mmol) was dissolved in THF (25 mL) and added dropwise into the mixture under rapid stirring. After that, the solution was stirred at 60 °C for 20 h under an argon atmosphere. After cooling down, the product was purified by flash chromatography (DCM:CH_3OH, 10:1), then filtered and dried in *vacuo*. Yield: 1.5 g, 56%. ^1H NMR (500 MHz, $CDCl_3$): δ 7.65 (s, 2H), 7.01 (m, 2H), 6.98 (m, 2H), 4.08 (t, 4H), 3.71 (t, 4H), 3.54 - 3.60 (m, 28H).

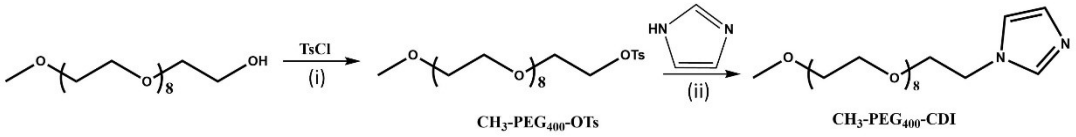

Scheme S2. Reaction conditions: (i) TsCl, TEA, DCM, 0 °C; (ii) imidazole, NaH, THF, 60 °C.

Synthesis of CH_3-PEG_{400}-OTs: CH_3-PEG_{400}-OTs was synthesized by following the

similar procedure of PEG_{400}-OTs_2 as mentioned above. ^1H NMR (500 MHz, $CDCl_3$): δ 7.78 (s, 1H), 7.34 (t, 2H), 4.10 (t, 2H), 3.62 (t, 2H), 3.59 - 3.51 (m, 30H), 3.47 (t, 2H), 3.31 (s, 3H), 2.38 (s, 3H).

Synthesis of CH_3-PEG_{400}-CDI: CH_3-PEG_{400}-CDI was synthesized by following the similar procedure of PEG_{400}-CDI_2 as mentioned above. ^1H NMR (500 MHz, $CDCl_3$): δ 7.39 (s, 1H), 6.86 (d, 2H), 3.96 (t, 2H), 3.59 (t, 2H), 3.52 - 3.40 (m, 30H), 3.39 (t, 2H), 3.21 (s, 3H).

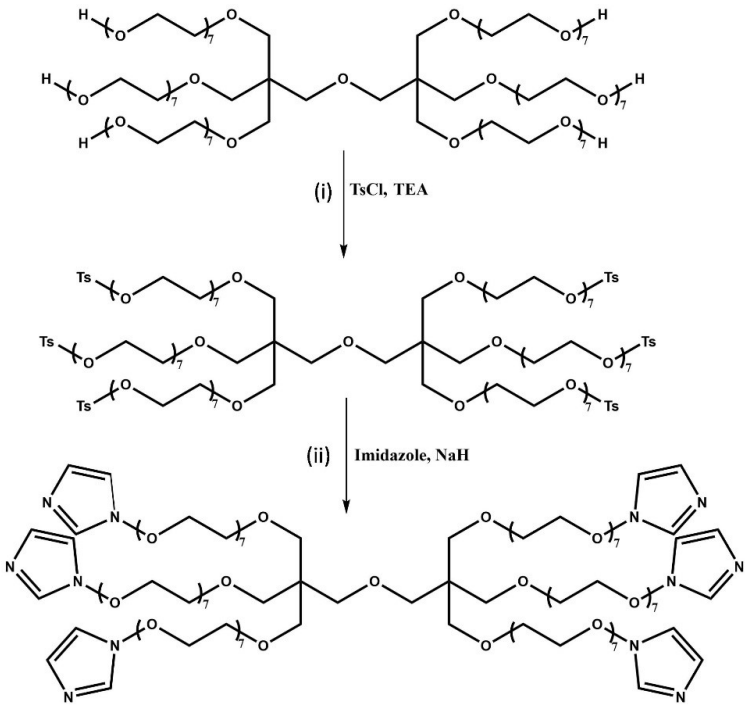

Scheme S3. Reaction conditions: (i) TsCl, TEA, DCM, 0 °C; (ii) imidazole, NaH, THF, 60 °C.

Synthesis of 6 arms-PEG_{2k}-OTs: 6 arms-PEG_{2k}-OTs was synthesized by following the similar procedure of PEG_{400}-OTs_2 as mentioned above. ^1H NMR (500 MHz, $CDCl_3$): δ 7.79 (d, 12H), 7.32 (d, 12H), 4.15 (t, 12H), 3.67 (t, 12H), 3.64 - 3.57 (m, 168H), 2.44 (s, 18H).

Synthesis of 6 arms-PEG_{2k}-CDI: 6 arms-PEG_{2k}-CDI was synthesized by following the similar procedure of PEG_{400}-CDI_2 as mentioned above. ^1H NMR (500 MHz, $CDCl_3$): δ 7.65 (s, 6H), 7.01 (d, 6H), 6.98 (d, 6H), 4.10 (t, 12H), 3.73 (t, 12H), 3.62 - 3.53 (m, 168H).

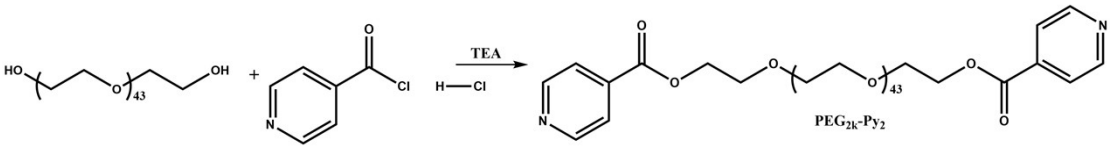

Scheme S4. Reaction conditions: isonicotinoyl chloride hydrochloride, TEA, DCM, 45 °C.

Synthesis of PEG_{2k}-Py_2: PEG_{2k} (7.0 g, 3.5 mmol) and isonicotinoyl chloride hydrochloride (1.0 g, 7.0 mmol) were dissolved in DCM (80 mL). TEA (1.06 g, 12.0 mmol) was dissolved in DCM (25 mL) and added dropwise into the mixture under rapid stirring. The solution was stirred at 45 °C for 20 h. After cooling down, the crude residue was purified by flash chromatography (DCM; DCM:CH_3OH, 19:1), then filtered and dried in *vacuo*. Yield: 4.0 g, 52%. ^1H NMR (500 MHz, $CDCl_3$): δ 8.79 (d, 4H), 7.89 (d, 4H), 4.52 (t, 4H), 3.84 (t, 4H), 3.70 - 3.59 (m, 172H).

3.2 Synthesis of Rhodium-based metal-organic polyhedra (Rh-MOP)

The Rh-MOP was synthesized following reported protocols.[4,5] A flask was charged with 5-hydroxyisophthalicacid (180 mg, 0.96 mmol), Na_2CO_3 (105 mg, 1 mmol) and rhodium (II) acetate dimer (100 mg, 0.23 mmol). 7 mL of dimethylacetamide (DMA) was introduced as solvent. The flask was then heated at 100 ºC for 48 h. The resulting precipitate was filtered from the reaction mixture and washed with DMA, acetone and chloroform respectively. Finally, the residue was dried in vacuo until constant weight.

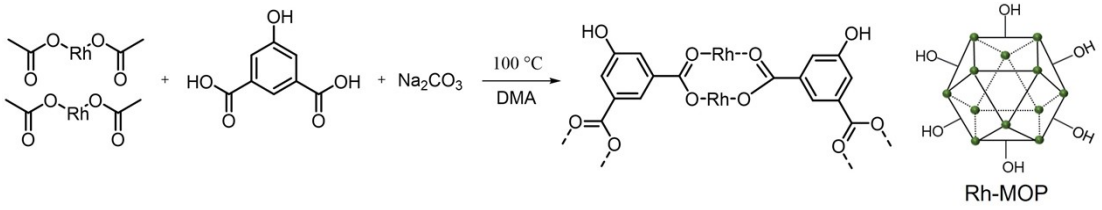

Scheme S5. Reaction conditions: rhodium (II) acetate dimer, 5-hydroxyisophthalicacid, $NaCO_3$, DMA, 100 °C.

3.3 Preparation of MOP hydrogels

Rh-MOP was dispersed in deionized water with 24 molar equivalents NaOH (1 M) and stirred at RT until the solution became homogeneous.[6] Telechelic ligands were dissolved in deionized water. MOP hydrogels were prepared by mixing the Rh-MOP

solutions and telechelic ligands solutions in different concentrations and stirring vigorously by the vortex, then standing or heating the mixture at 50~80 ℃ for several hours.

Taking MOP-PEG_{400} hydrogels as an example: Rh-MOP (22.4 mg, 3.36×10^{-3} mmol) was dispersed in deionized water (1.2 mL) with 24 molar equivalents NaOH (1 M) and stirred at RT until the green solution became homogeneous. PEG_{400}-CDI_2 (16.1 mg, 4.32×10^{-2} mmol) was dissolved in deionized water (1.2 mL). MOP-PEG_{400} hydrogels were prepared by mixing the Rh-MOP solutions and PEG_{400}-CDI_2 solutions and stirring vigorously by the vortex, then heating the mixture at 60 ℃ for 1 h.

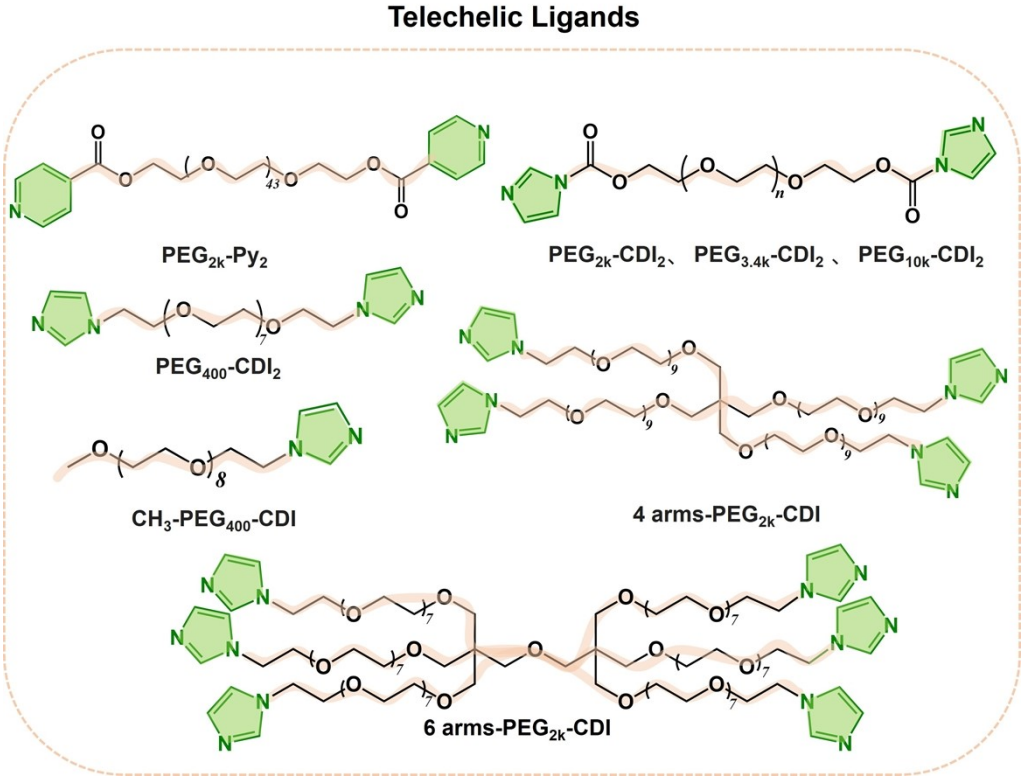

Fig. S1 Molecular formula of different kinds of telechelic ligands.

3.4 Preparation of MOP aerogels

The MOP hydrogel was soaked in deionized water for one week to remove uncoordinated Rh-MOP and imidazole-based functionalized ligands in the hydrogel systems, then the MOP hydrogels were pre-frozen in a liquid nitrogen bath for 1 h, and put it into a freeze dryer for 48 h to freeze-dry to obtain MOP aerogels.

3.5 Adsorption experiments

Iodine is dissolved in water to prepare aqueous iodine solution with concentration of 1 mM. Before the adsorption test, the structural and dimensional stability of the MOP hydrogels are demonstrated. Iodine adsorption experiments are conducted by soaking the MOP hydrogels (100 μL) into 2 mL 1 mM iodine aqueous solution at room temperature. UV-vis spectroscopy is exploited to monitor the adsorption processes. The supernatant solution is extracted at various time and the UV-vis data is subsequently recorded. The characteristic absorption centered at 460 nm is selected as the reference peak, and the absorbance intensity of the raw iodine solution is normalized to 100%.

The removal ratios (R) of iodine were calculated using $R = (C_0 – C_t) / C_0 \times 100\%$ (where C_0 and C_t represent the initial concentration and concentration at time *t* of aqueous iodine solution, respectively).

The amount of adsorbed iodine was determined using the following aquation: $q_t = (C_0 – C_t)\ Mw / m \times 1000$ (where q_t (g g^{-1}) is amount of iodine adsorbed per g of adsorbent at time *t* (min). C_0 and C_t represent the initial concentration and concentration at time *t* of aqueous iodine solution, respectively; *m* (g) is the mass of adsorbent used in the study. *Mw* (g mol^{-1}) is the molar mass of iodine).

The adsorption kinetics were quantified using Ho and McKay's pseudo-second-order model, $k = (q_t – q_0) / t$ (where q_t (g g^{-1}) and q_0 (g g^{-1}) is amount of iodine adsorbed per g of adsorbent at time *t* (min) and the initial time, respectively.)

4. Supplementary Figures and Tables

4.1 Supplementary figures

Fig. S2 The structure characterization of Rh-MOP.

Fig. S3 Mechanical properties of MOP hydrogels.

Fig. S4 Mechanical properties of MOP-4 arms-PEG_{2k} hydrogels.

Fig. S5 Mechanical properties of MOP-6 arms-PEG_{2k} hydrogels.

Fig. S6 Mechanical properties of MOP-PEG_{400} hydrogels.

Fig. S7 Mechanical properties of MOP-$PEG_{3.4k}$ hydrogels.

Fig. S8 Time-resolved correlation function data confirms the solution-gel transition upon the mixing of Rh-MOP and 4 arms-PEG_{2k}-CDI precursors in solution.

Fig. S32 Time-dependent UV-vis adsorption spectra of iodine solutions (1 mM) upon addition of $PEGDA_{1k}$ hydrogels system.

Fig. S33 Time-dependent UV-vis adsorption spectra of iodine solutions (1 mM) upon addition of Rh-MOP.

Fig. S34 Time-dependent UV-vis adsorption spectra of iodine solutions (1 mM) upon addition of MOP-PEG_{2k} hydrogels system.

Fig. S35 Time-dependent UV-vis adsorption spectra of iodine solutions (1 mM) upon addition of MOP-4 arms-PEG_{2k} hydrogels system.

Fig. S36 Time-dependent UV-vis adsorption spectra of iodine solution (1 mM) upon addition of MOP-6 arms-PEG_{2k} hydrogels was run for 1.5 min each cycle and repeated 7 times.

Fig. S37 Photographs of MOP hydrogels under prolonged immersion in aqueous solution after iodine solution (1 mM) adsorption.

Fig. S38 UV-vis spectra of MOP hydrogels under prolonged immersion in aqueous solution after iodine solution (1 mM) adsorption.

Fig. S39 ^1H NMR spectra of PEG_{400}-OTs_2 in $CDCl_3$ at 298 k.

Fig. S40 ^1H NMR spectra of PEG_{400}-CDI_2 in $CDCl_3$ at 298 k.

Fig. S41 ^1H NMR spectra of CH_3-PEG_{400}-OTs in $CDCl_3$ at 298 k.

Fig. S42 ^1H NMR spectra of CH_3-PEG_{400}-CDI in $CDCl_3$ at 298 k.

Fig. S43 ^1H NMR spectra of 6 arms-PEG_{2k}-OTs in $CDCl_3$ at 298 k.

Fig. S44 ^1H NMR spectra of 6 arms-PEG_{2k}-CDI in $CDCl_3$ at 298 k.

Fig. S45 ^1H NMR spectra of PEG_{2k}-Py_2 in $CDCl_3$ at 298 k.

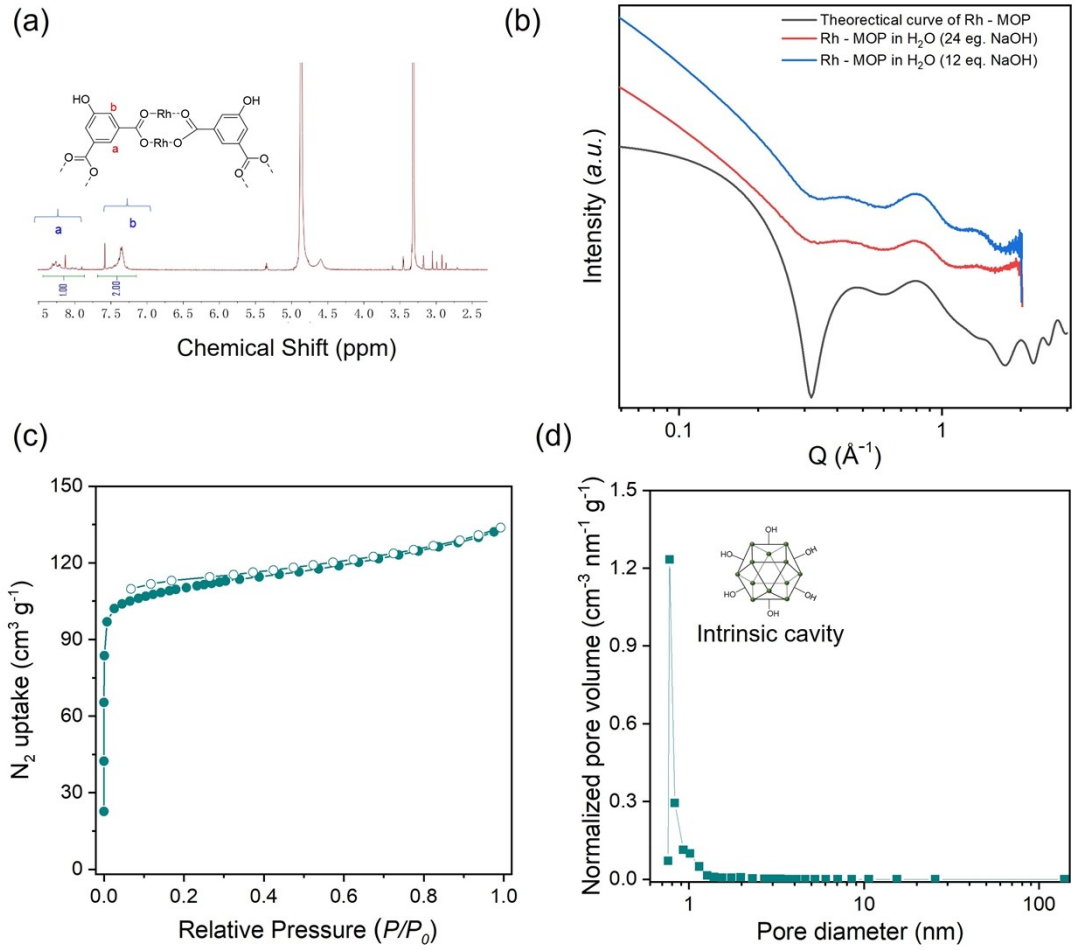

Fig. S2 (a) ^{1}H NMR spectrum of Rh-MOP in methanol-d_4. (b) Experimental WAXS curves of the deprotonated Rh-MOP and theoretical WAXS curve of the Rh-MOP. (c) N_2 adsorption isotherm of Rh-MOP at 77 K showed rapid adsorption at low pressure region, characteristics of the adsorption behavior for typical microporous materials. (d) Normalized pore size distributions of Rh-MOP calculated from the adsorption data by employment of the DFT method.

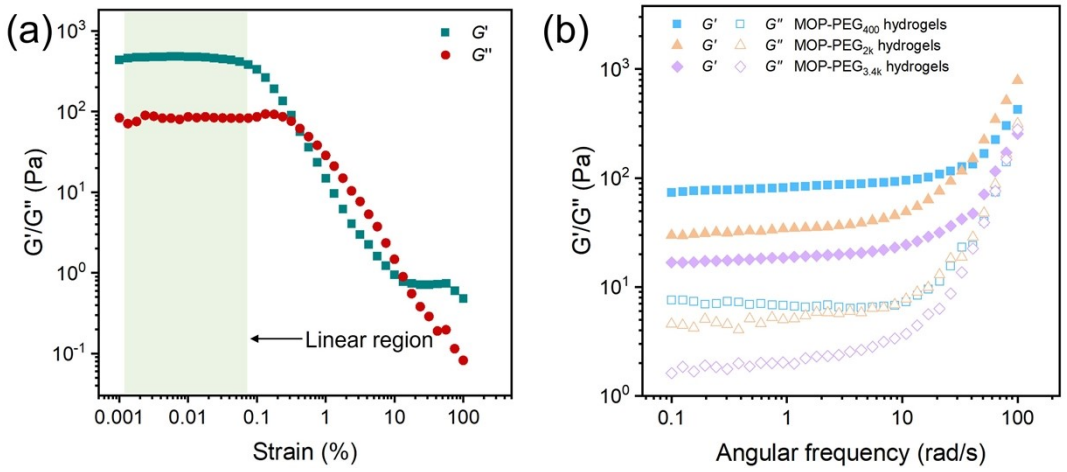

Fig. S3 Mechanical properties of MOP hydrogels. (a) Amplitude sweep data of MOP-PEG_{2k} hydrogels. (b) Frequency sweep data of MOP hydrogels.

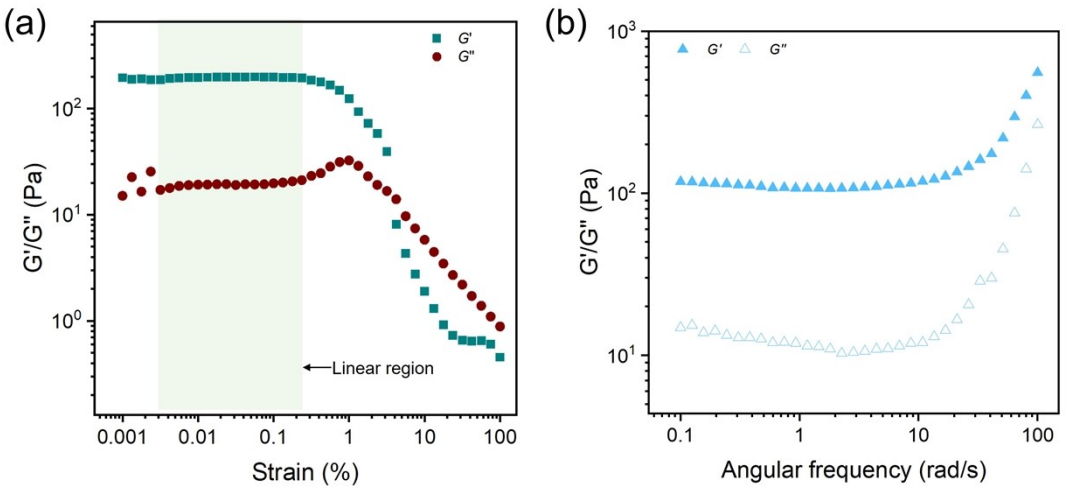

Fig. S4 Mechanical properties of MOP-4 arms-PEG_{2k} hydrogels. (a) Amplitude sweep data (25 °C, ω = 5 rad s^{-1}). (b) Frequency sweep data (25 °C, γ = 0.01%).

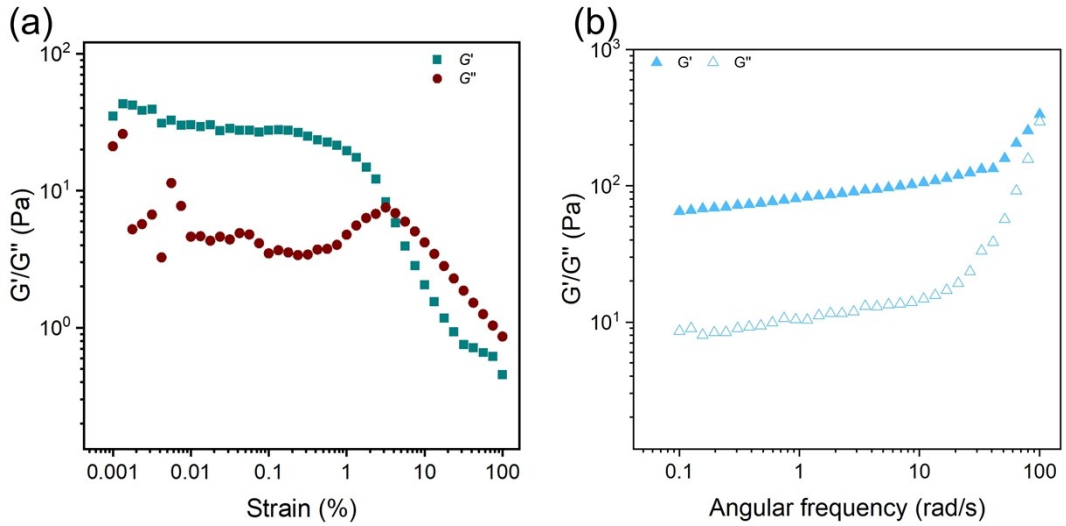

Fig. S5 Mechanical properties of MOP-6 arms-PEG_{2k} hydrogels. (a) Amplitude sweep data (25 °C, ω = 5 rad s^{-1}). (b) Frequency sweep data (25 °C, γ = 0.01%).

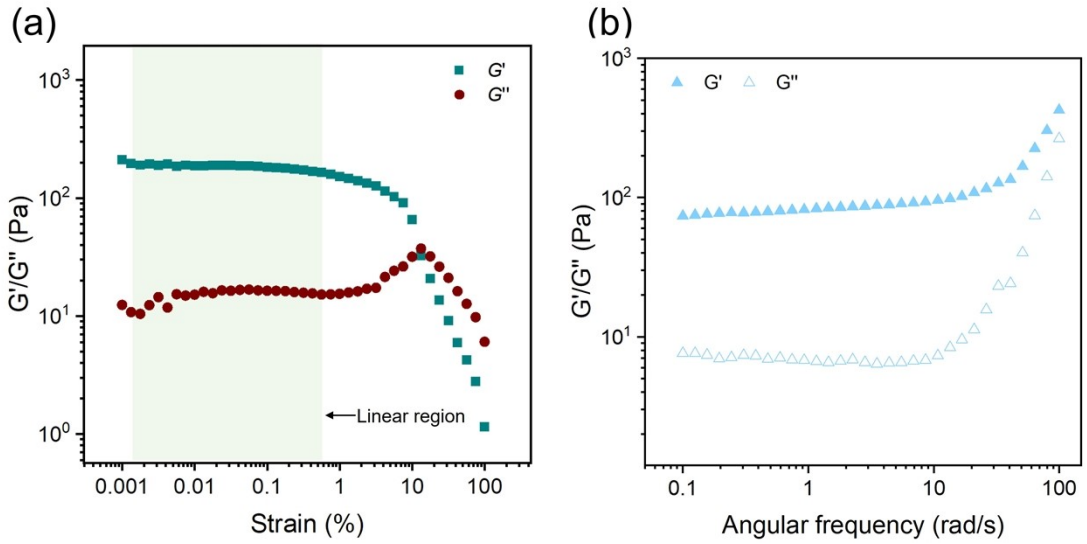

Fig. S6 Mechanical properties of MOP-PEG_{400} hydrogels. (a) Amplitude sweep data (25 °C, ω = 5 rad s^{-1}). (b) Frequency sweep data (25 °C, γ = 0.1%).

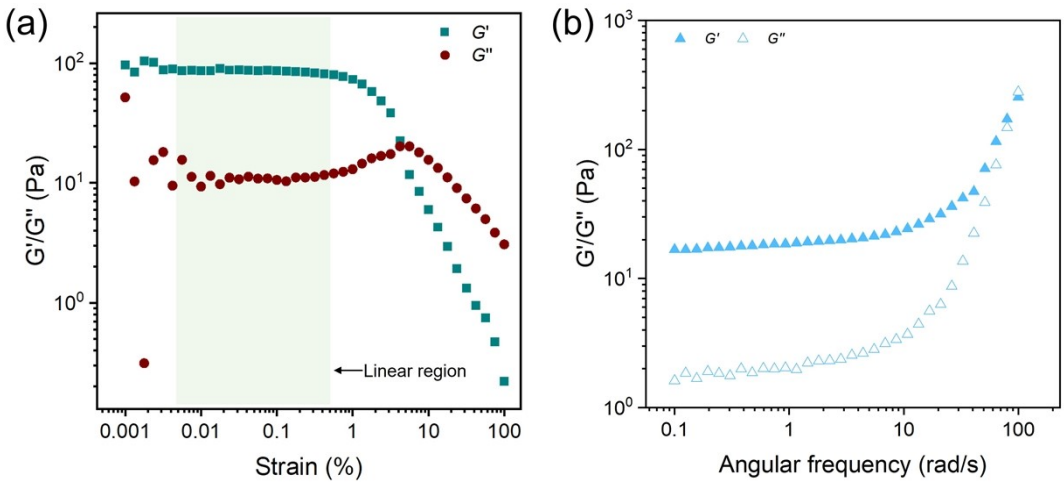

Fig. S7 Mechanical properties of MOP-PEG$_{3.4k}$ hydrogels. (a) Amplitude sweep data (25 °C, ω = 5 rad s^{-1}). (b) Frequency sweep data (25 °C, γ = 0.1%).

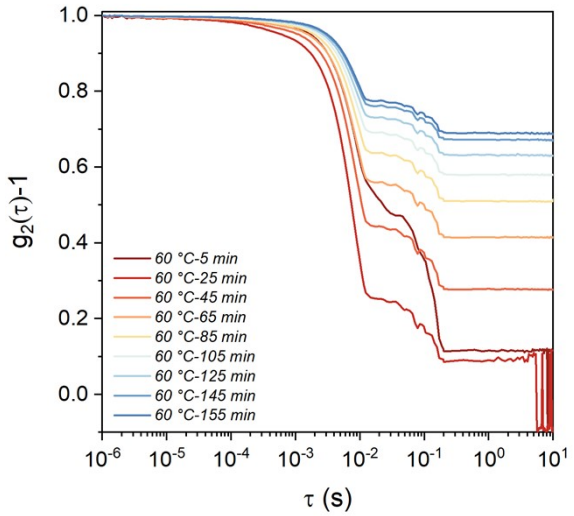

Fig. S8 Time-resolved correlation function data confirms the solution-gel transition upon the mixing of Rh-MOP and 4 arms-PEG$_{2k}$-CDI precursors in solution.

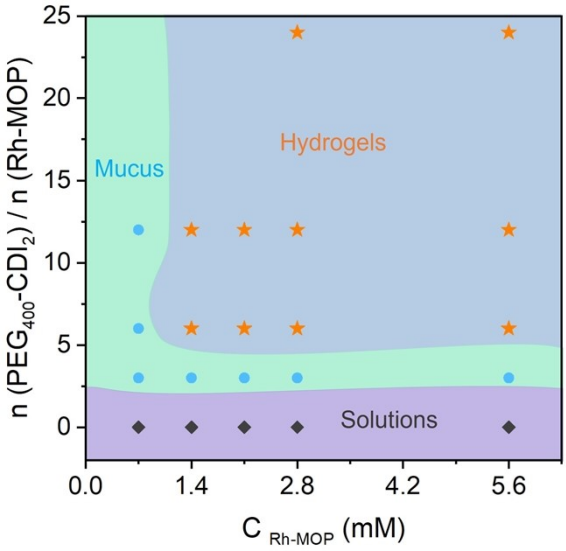

Fig. S9 Binary phase diagram of Rh-MOP-PEG_{400}-CDI_2 systems (Mucus (blue dot), solutions (black diamond), hydrogels (orange star)). The specific result is listed at Table S2.

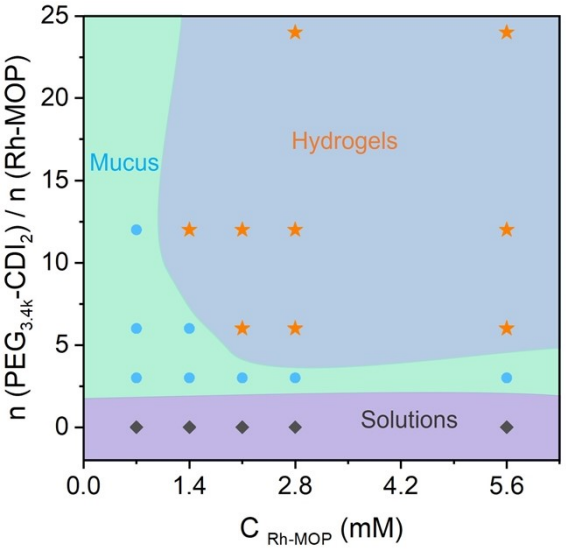

Fig. S10 Binary phase diagram of Rh-MOP-$PEG_{3.4k}$-CDI_2 systems (Mucus (blue dot), solutions (black diamond), hydrogels (orange star)). The specific result is listed at Table S3.

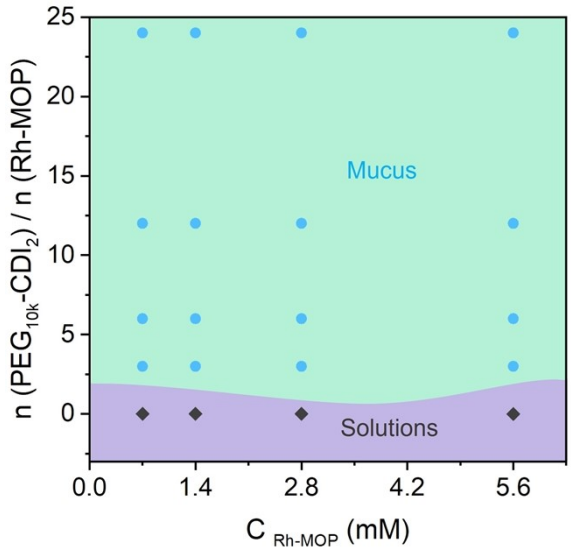

Fig. S11 Binary phase diagram of Rh-MOP-PEG_{10k}-CDI_2 systems (Mucus (blue dot), solutions (black diamond)). The specific result is listed at Table S4.

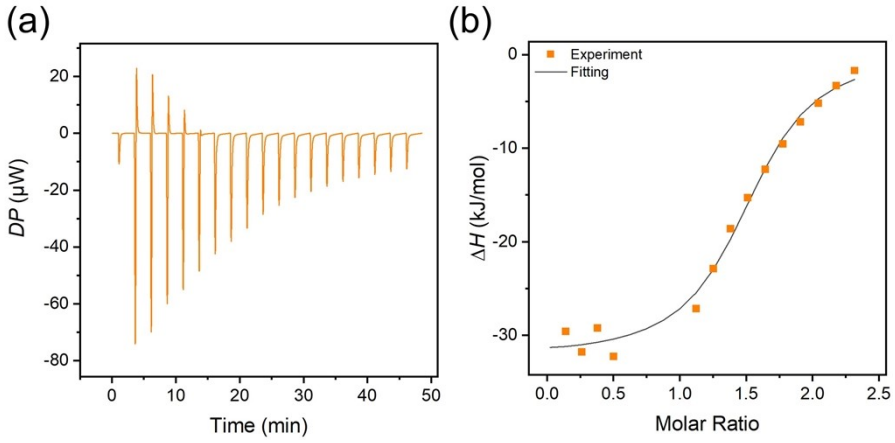

Fig. S12 (a) ITC titration results of MOP and PEG_{2k}-Py_2 systems. (b) ITC fitting curve of MOP and PEG_{2k}-Py_2 systems. The specific result is listed at Table S7.

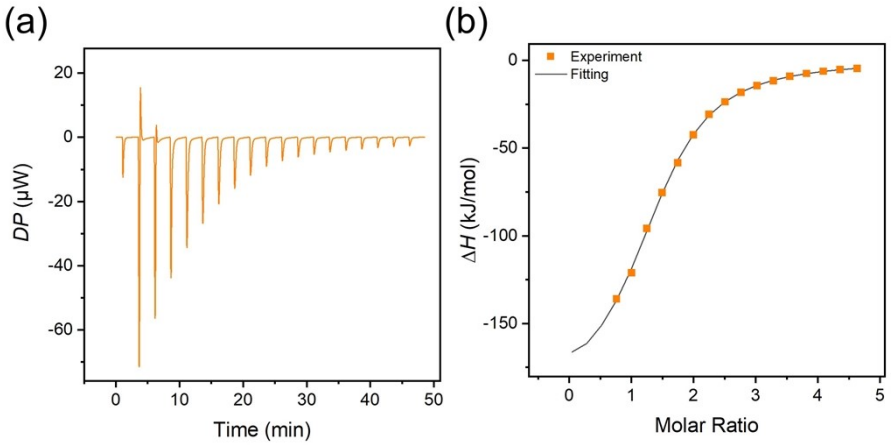

Fig. S13 (a) ITC titration results of MOP and PEG_{400}-CDI_2 systems. (b) ITC fitting curve of MOP and PEG_{400}-CDI_2 systems. The specific result is listed at Table S7.

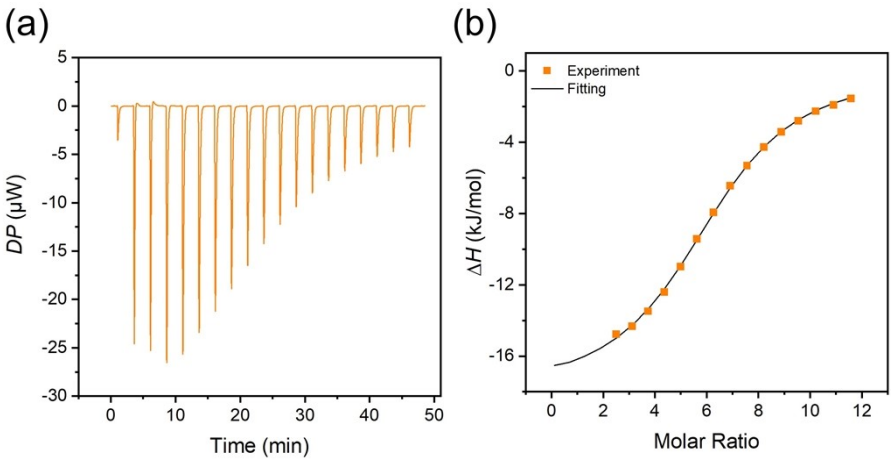

Fig. S14 (a) ITC titration results of MOP and $PEG_{3.4k}$-CDI_2 systems. (b) ITC fitting curve of MOP and $PEG_{3.4k}$-CDI_2 systems. The specific result is listed at Table S7.

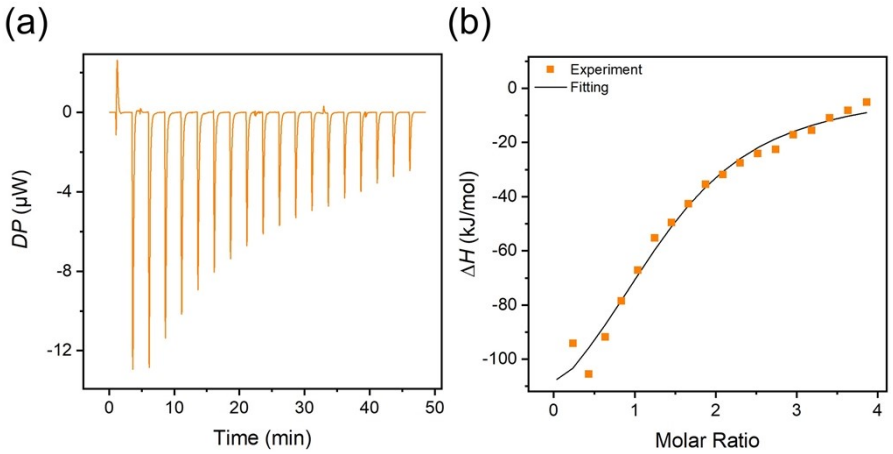

Fig. S15 (a) ITC titration results of MOP and PEG_{10k}-CDI_2 systems. (b) ITC fitting curve of MOP and PEG_{10k}-CDI_2 systems. The specific result is listed at Table S7.

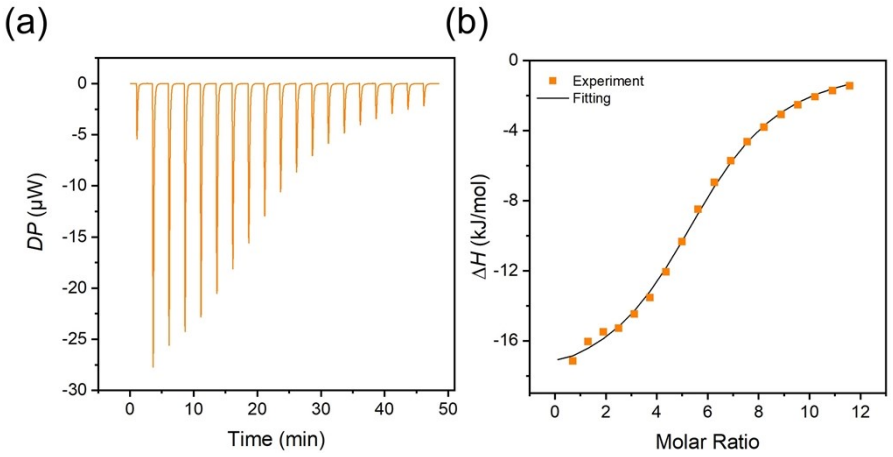

Fig. S16 (a) ITC titration results of MOP and CH_3-PEG_{400}-CDI systems. (b) ITC fitting curve of MOP and CH_3-PEG_{400}-CDI systems. The specific result is listed at Table S7.

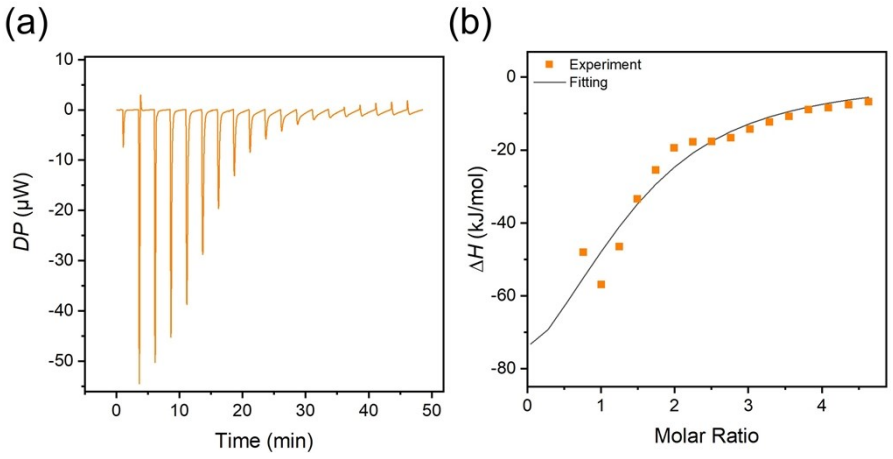

Fig. S17 (a) ITC titration results of MOP and 4 arms-PEG_{2k}-CDI systems. (b) ITC fitting curve of MOP and 4 arms-PEG_{2k}-CDI systems. The specific result is listed at Table S7.

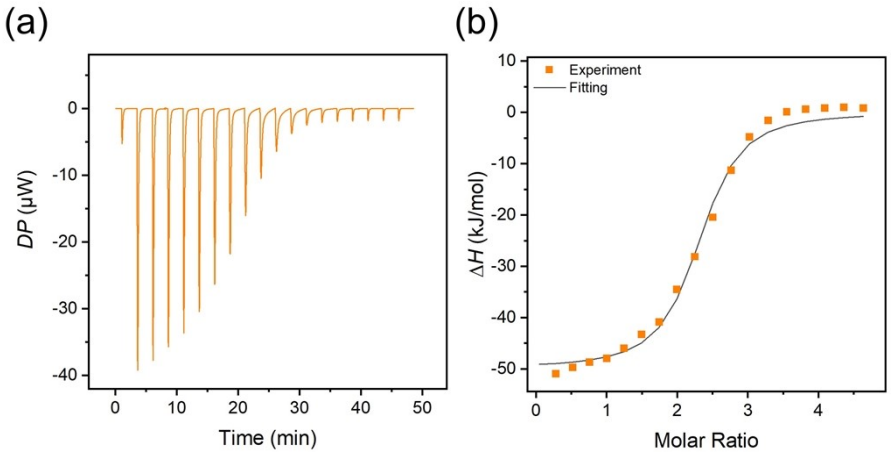

Fig. S18 (a) ITC titration results of MOP and 6 arms-PEG_{2k}-CDI systems. (b) ITC fitting curve of MOP and 6 arms-PEG_{2k}-CDI systems. The specific result is listed at Table S7.

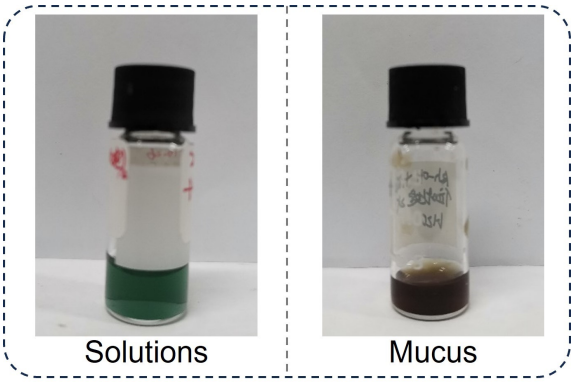

Fig. S19 Photographs of MOP-PEG_{2k}-Py_2 systems.

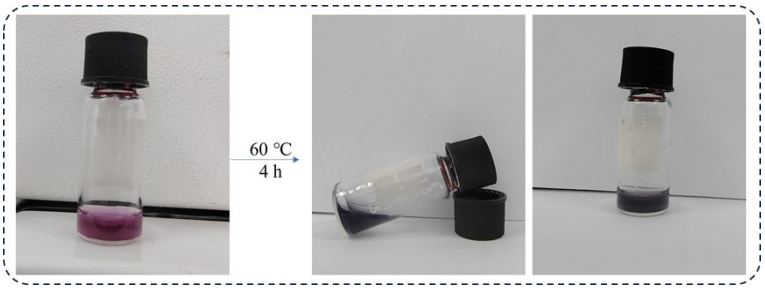

Fig. S20 Photographs of MOP-PEG_{10k} systems.

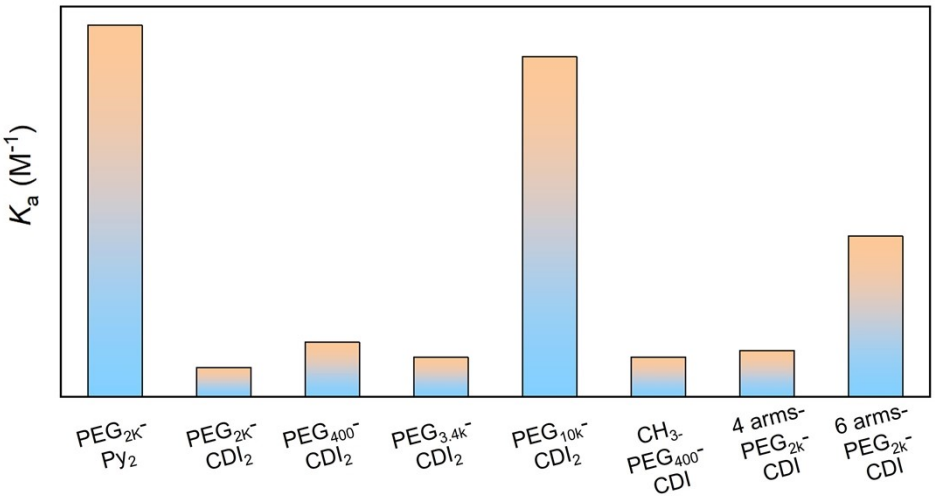

Fig. S21 Binding constants (*K*a) between Rh-MOP and the PEG ligands.

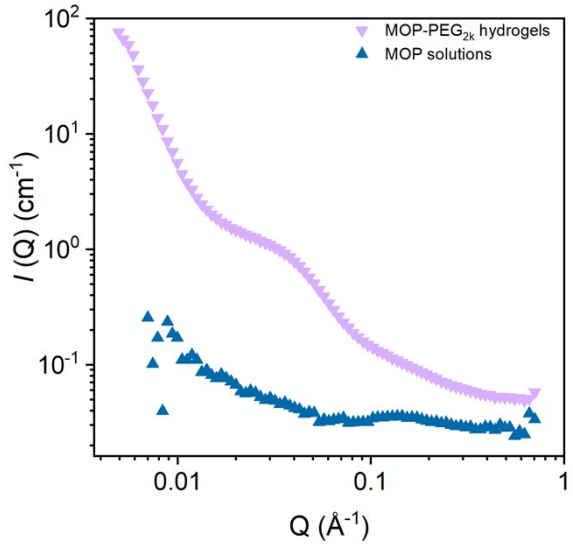

Fig. S22 SANS data of MOP-PEG_{2k} hydrogels and MOP solutions.

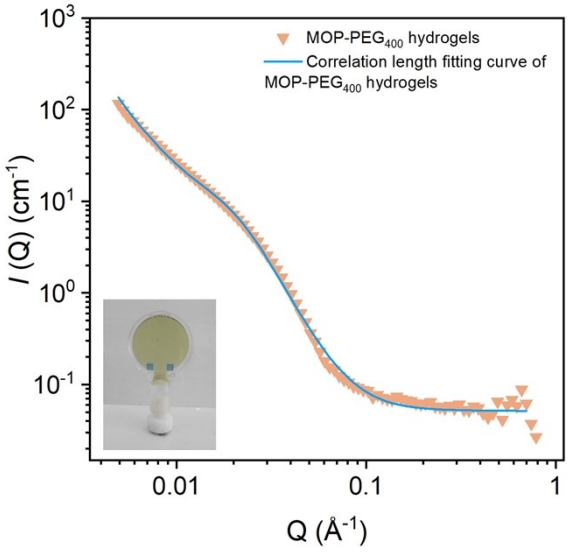

Fig. S23 SANS data and photograph of MOP-PEG_{400} hydrogels and the fitting profile based on correlation length model.

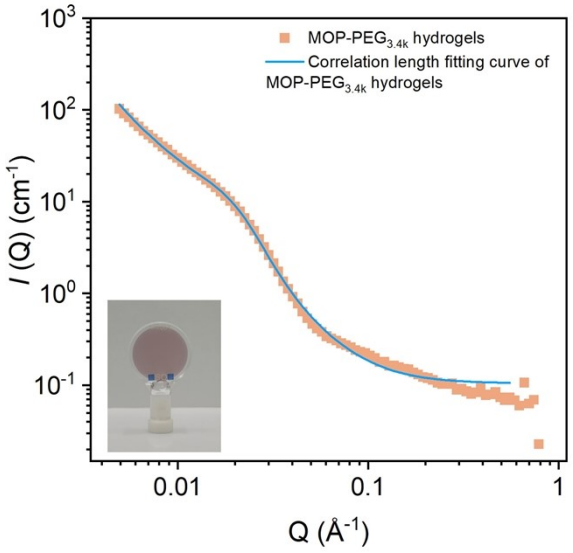

Fig. S24 SANS data and photograph of MOP-PEG$_{3.4k}$ hydrogels and the fitting profile based on correlation length model.

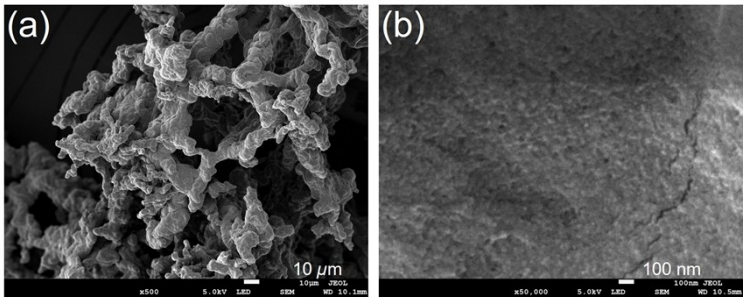

Fig. S25 Morphological studies of MOP-4 arms-PEG$_{2k}$ hydrogels. (a)-(b) SEM images of the freeze-dried MOP-4 arms-PEG$_{2k}$ hydrogels.

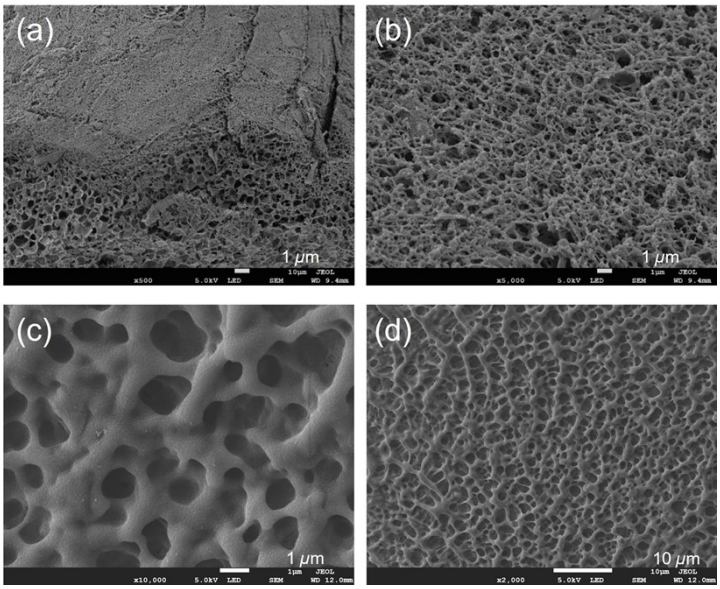

Fig. S26 (a), (b) SEM images of the freeze-dried MOP-6 arms-PEG_{2k} system. (c), (d) Cryo-SEM images of the MOP-6 arms-PEG_{2k} system.

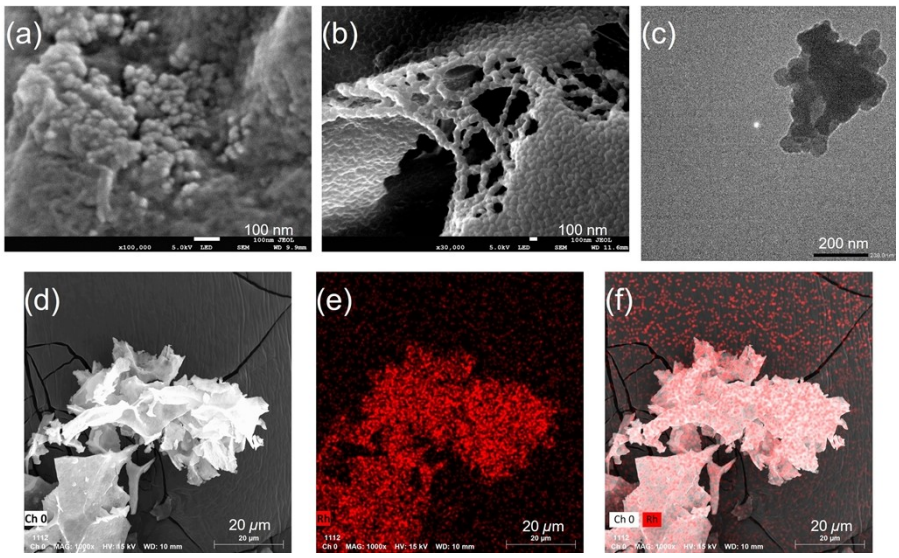

Fig. S27 Morphological studies of MOP-PEG_{400} hydrogels. (a) SEM image of the freeze-dried MOP-PEG_{400} hydrogels. (b) Cryo-SEM image of MOP-PEG_{400} hydrogels. (c) TEM image of freeze-dried MOP-PEG_{400} hydrogels. (d) SEM image of the freeze-dried MOP-PEG_{400} hydrogels (15 kV). (e) EDX images of the freeze-dried MOP-PEG_{400} hydrogels (red, Rh element). (f) SEM/EDX composite images of the freeze-dried MOP-PEG_{400} hydrogels.

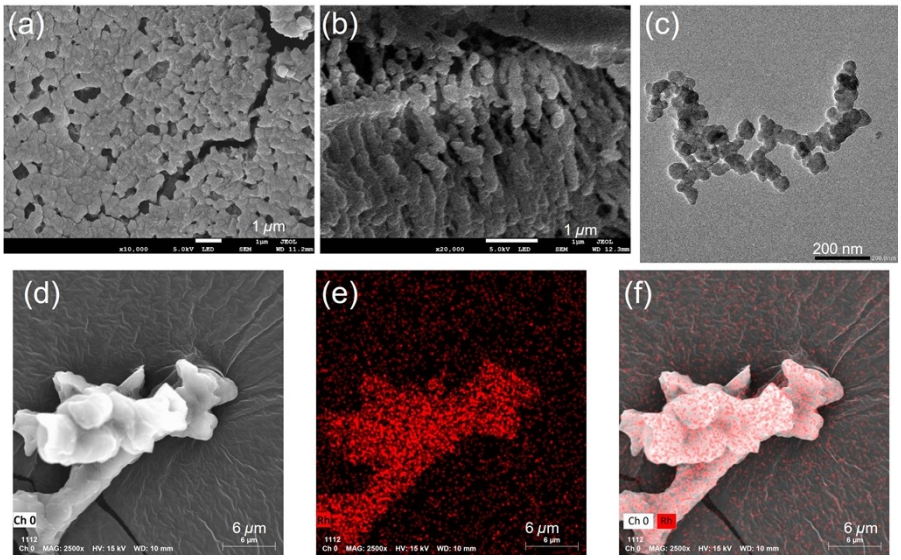

Fig. S28 Morphological studies of MOP-$PEG_{3.4k}$ hydrogels. (a) SEM image of the freeze-dried MOP-$PEG_{3.4k}$ hydrogels. (b) Cryo-SEM image of MOP-$PEG_{3.4k}$ hydrogels. (c) TEM image of freeze-dried MOP-$PEG_{3.4k}$ hydrogels. (d) SEM image of the freeze-dried MOP-$PEG_{3.4}$ hydrogels (15 kV). (e) EDX images of the freeze-dried MOP-$PEG_{3.4k}$ hydrogels (red, Rh element). (f) SEM/EDX composite images of the freeze-dried MOP-$PEG_{3.4k}$ hydrogels.

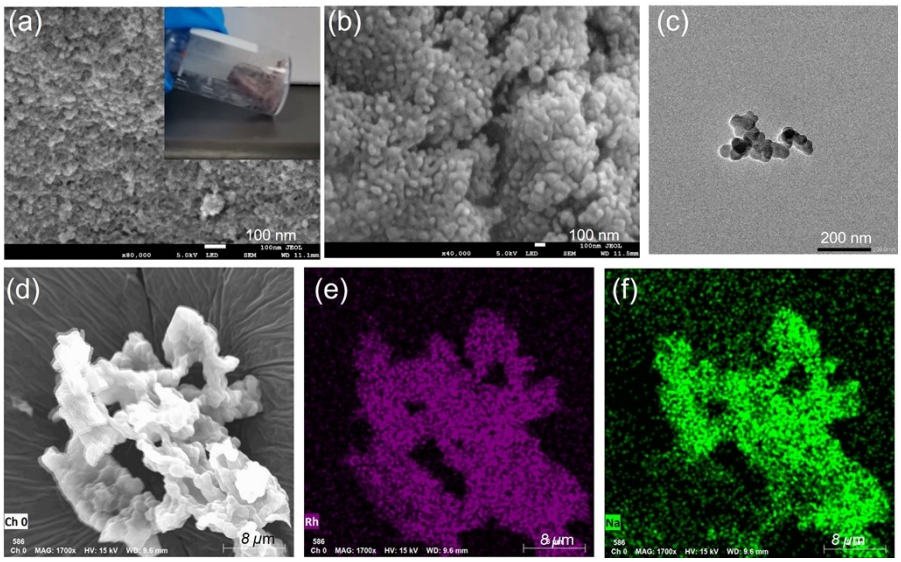

Fig. S29 (a) SEM image and photograph of the freeze-dried MOP-PEG_{2k} system. (b) Cryo-SEM image of MOP-PEG_{2k} system. (c) TEM image of freeze-dried MOP-PEG_{2k} system. (d) SEM image of the freeze-dried MOP-PEG_{2k} system (15 kV). (e), (f) EDX images of the freeze-dried MOP-PEG_{2k} system (purple, Rh element; green, Na element).

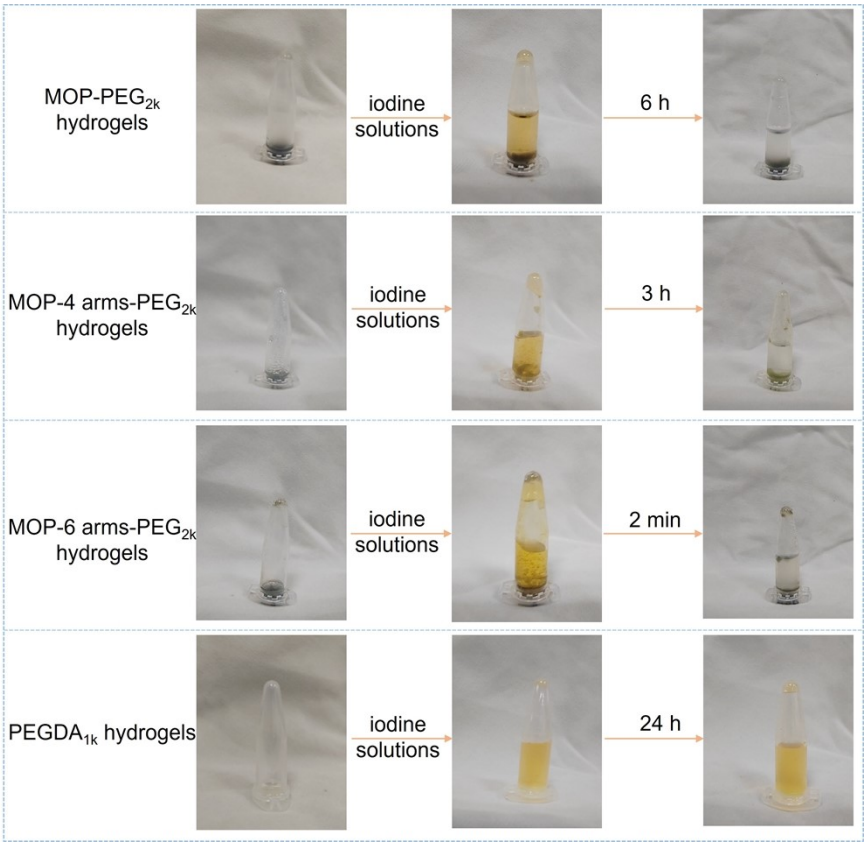

Fig. S30 Photographs of the color change of iodine (1 mM) in aqueous solution adsorbed by MOP hydrogels and $PEGDA_{1k}$ hydrogels.

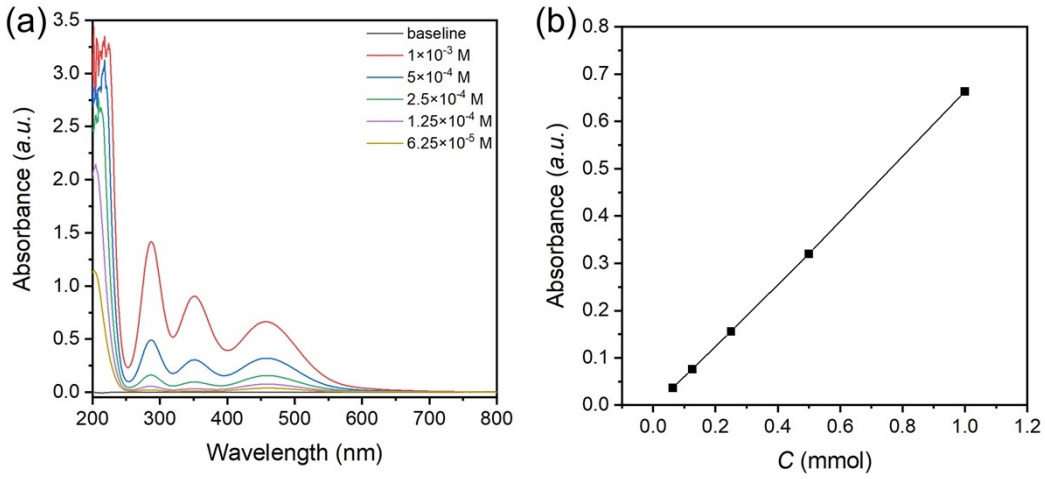

Fig. S31 (a) Iodine UV-vis spectrum and (b) calibration line performed with solutions of different concentrations of iodine (1 mM, 0.5 mM, 0.25 mM, 0.125 mM and 0.0625 mM). UV-vis test for iodine were measured at 460 nm.

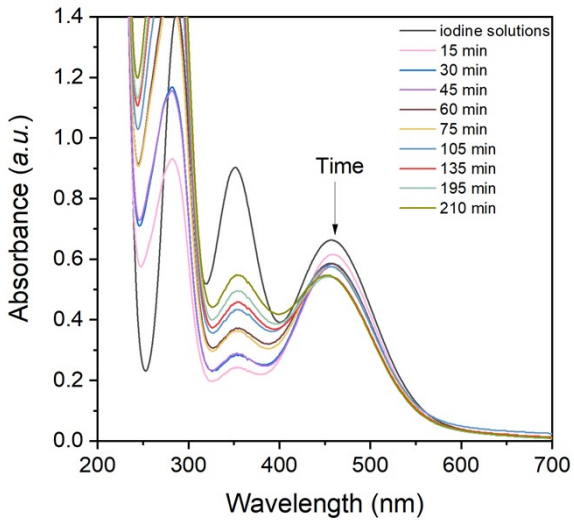

Fig. S32 Time-dependent UV-vis adsorption spectra of iodine solutions (1 mM) upon addition of $PEGDA_{1k}$ hydrogels system.

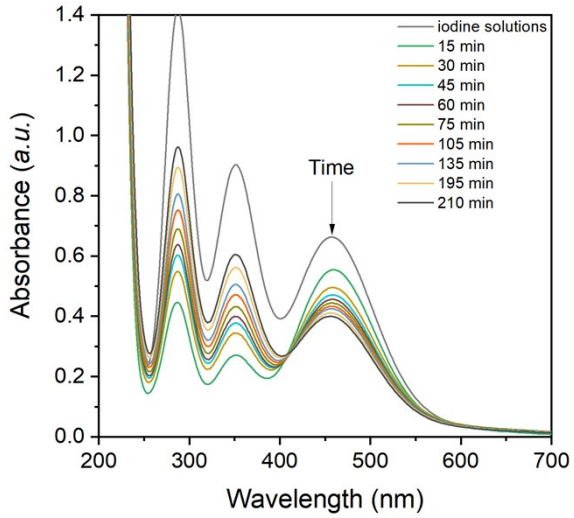

Fig. S33 Time-dependent UV-vis adsorption spectra of iodine solutions (1 mM) upon addition of Rh-MOP.

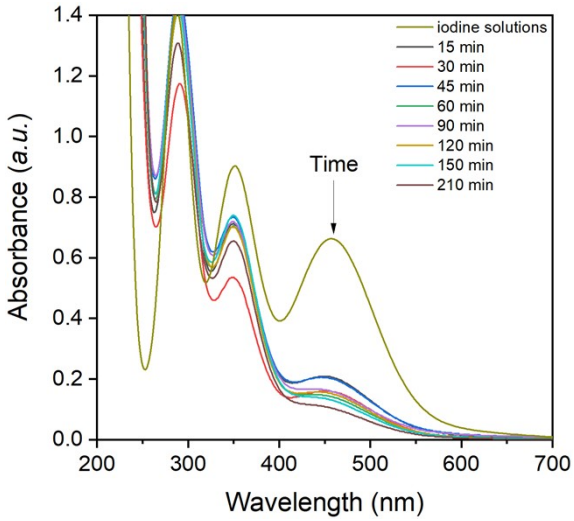

Fig. S34 Time-dependent UV-vis adsorption spectra of iodine solutions (1 mM) upon addition of MOP-PEG_{2k} hydrogels system.

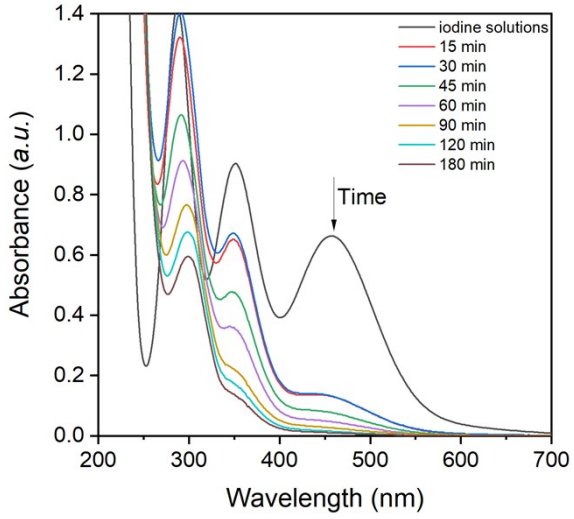

Fig. S35 Time-dependent UV-vis adsorption spectra of iodine solutions (1 mM) upon addition of MOP-4 arms-PEG_{2k} hydrogels system.

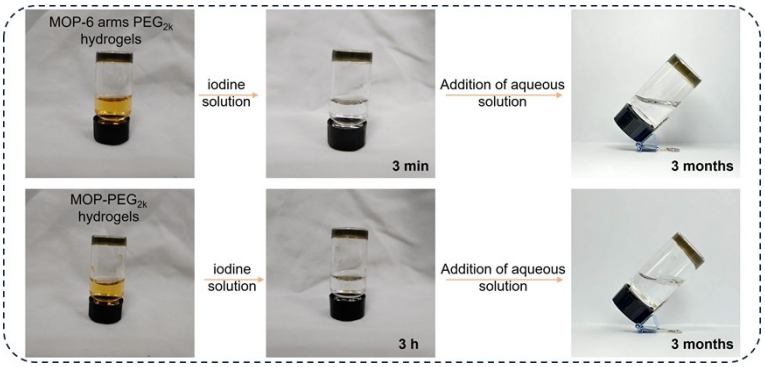

Fig. S36 Photographs of MOP hydrogels under prolonged immersion in aqueous solution after iodine solution (1 mM) adsorption.

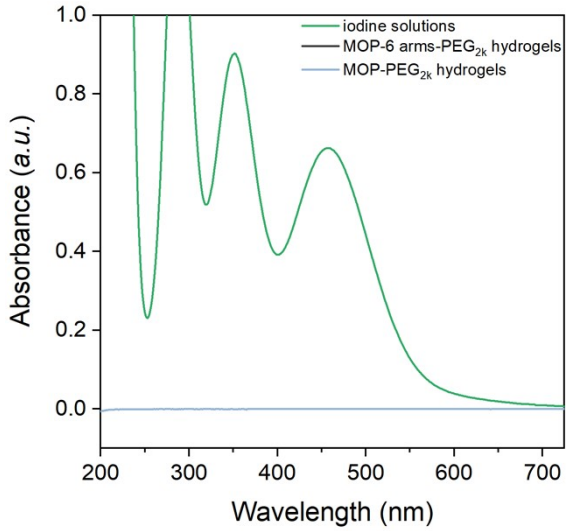

Fig. S37 UV-vis spectra of MOP hydrogels under immersion in aqueous solution after iodine solution (1 mM) adsorption for 3 months.

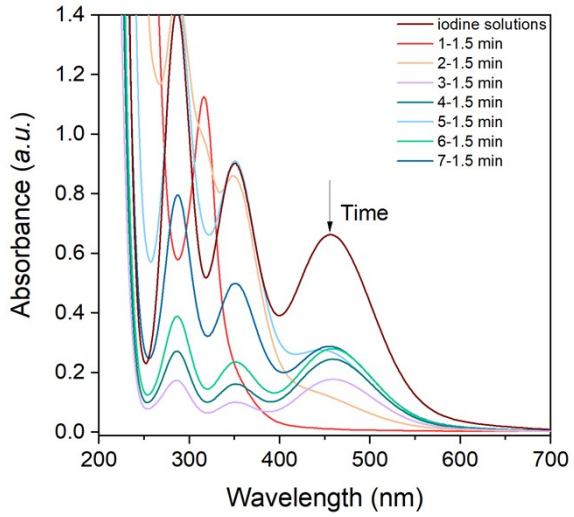

Fig. S38 Time-dependent UV-vis adsorption spectra of iodine solutions (1 mM) upon addition of MOP-6 arms-PEG_{2k} hydrogels was run for 1.5 min each cycle and repeated 7 times.

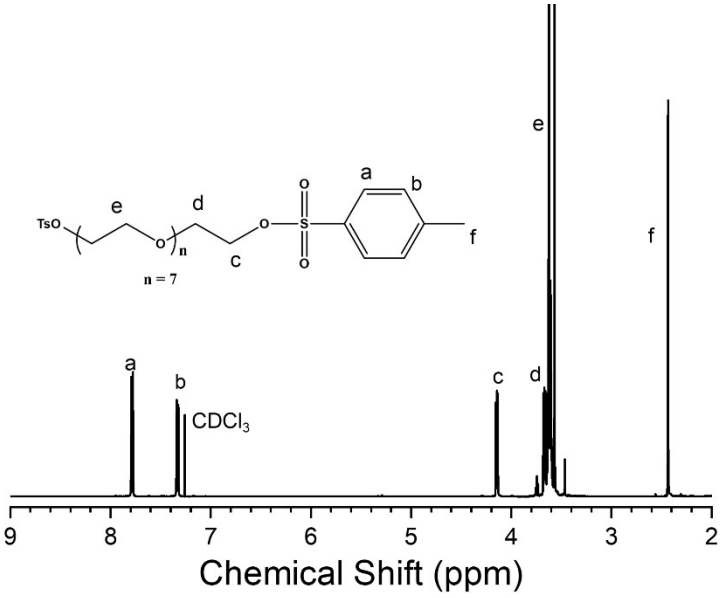

Fig. S39 ^{1}H NMR spectra of PEG_{400}-OTs_2 in $CDCl_3$ at 298 k.

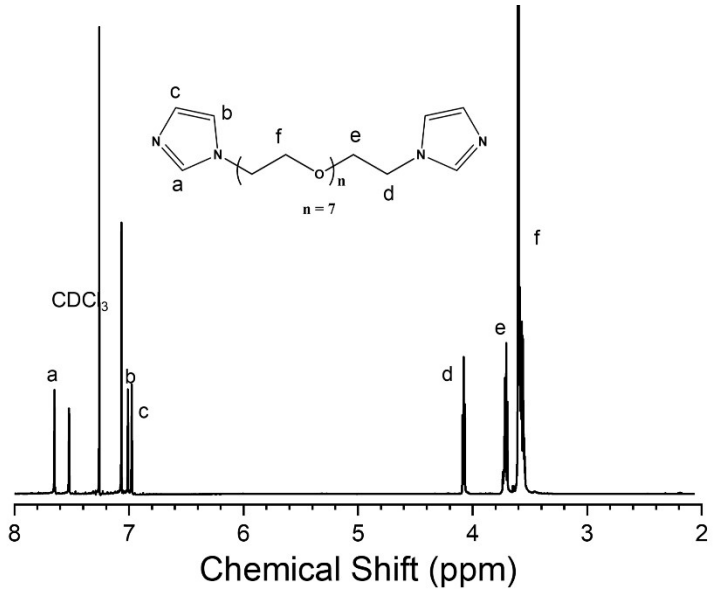

Fig. S40 ^{1}H NMR spectra of PEG_{400}-CDI_2 in $CDCl_3$ at 298 k.

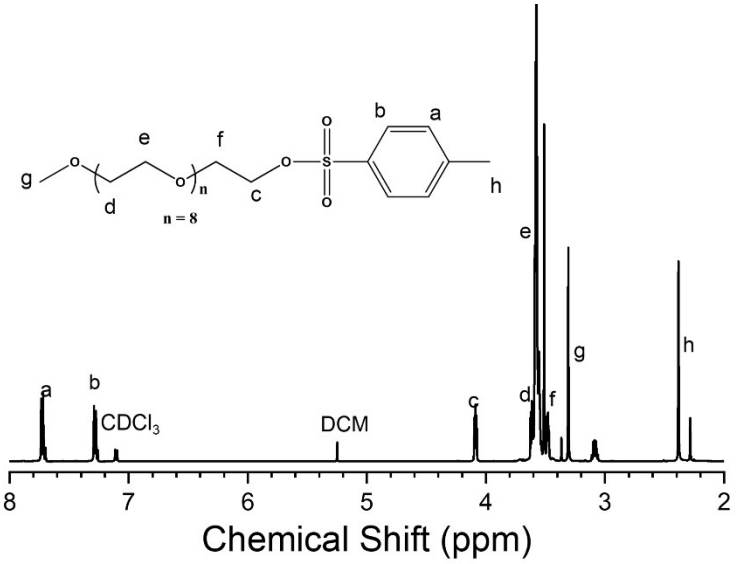

Fig. S41 ^{1}H NMR spectra of CH_3-PEG_{400}-OTs in $CDCl_3$ at 298 k.

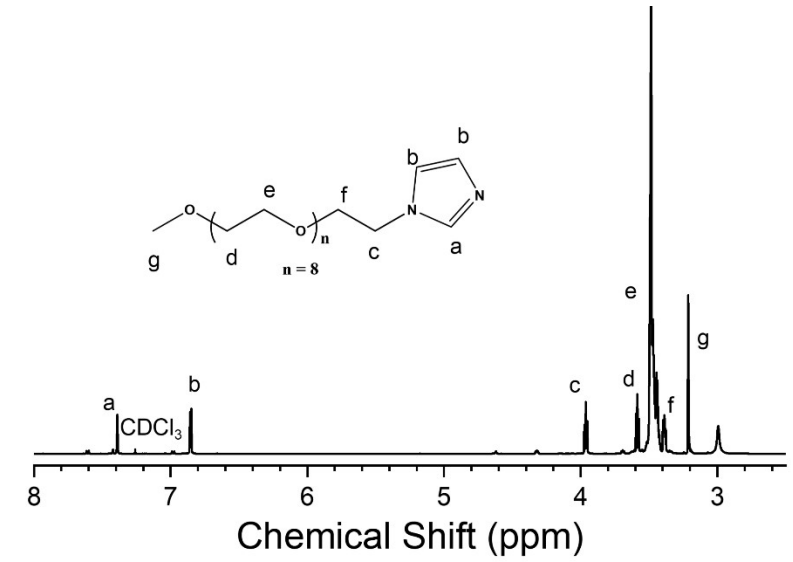

Fig. S42 ^{1}H NMR spectra of CH_3-PEG_{400}-CDI in $CDCl_3$ at 298 k.

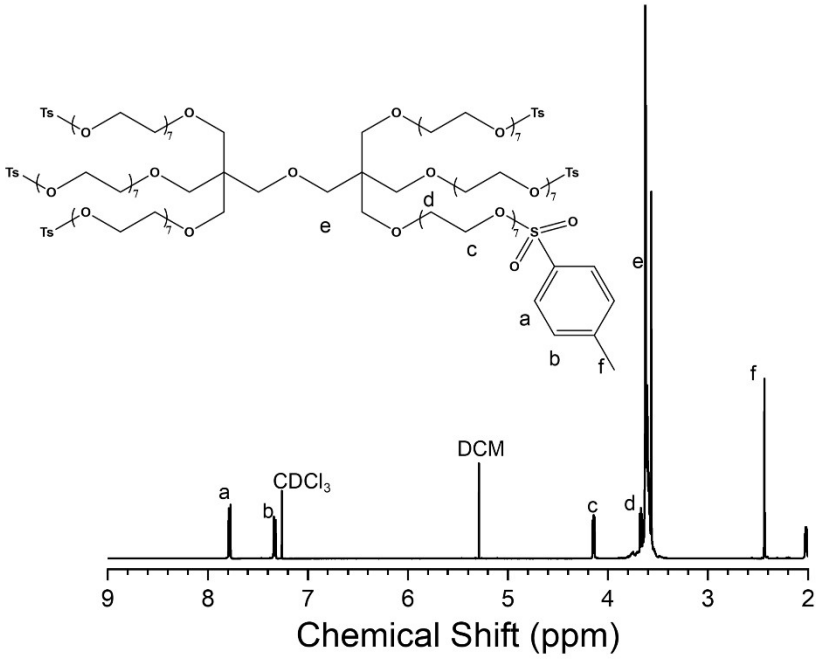

Fig. S43 ^{1}H NMR spectra of 6 arms-PEG_{2k}-OTs in $CDCl_3$ at 298 k.

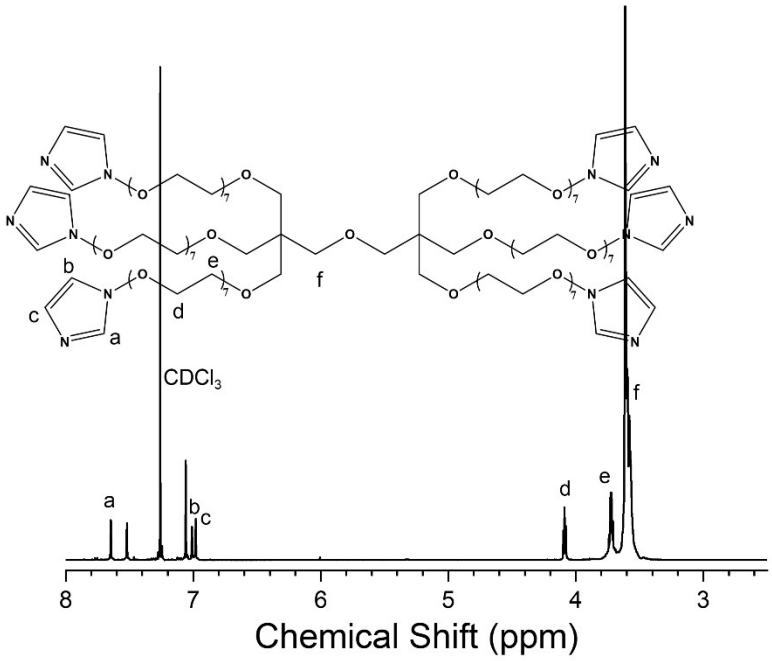

Fig. S44 ^{1}H NMR spectra of 6 arms-PEG_{2k}-CDI in $CDCl_3$ at 298 k.

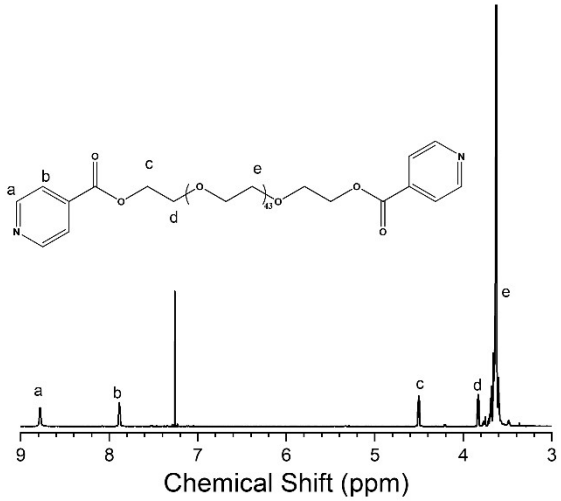

Fig. S45 ^{1}H NMR spectra of PEG_{2k}-Py_2 in $CDCl_3$ at 298 k.

4.2 Supplementary tables

Table S1. Gelation properties of MOP-PEG_{2k} systems

Table S2. Gelation properties of MOP-PEG_{400} systems

Table S3. Gelation properties of MOP-$PEG_{3.4k}$ systems

Table S4. Gelation properties of MOP-PEG_{10k} systems

Table S5. Gelation properties of MOP-4 arms-PEG_{2k} systems

Table S6. Gelation properties of MOP-6 arms-PEG_{2k} systems

Table S7. The thermos-behaviors of MOP and telechelic ligands

Table S8. List of iodine adsorption performances for different adsorbents in water environments

Table S1. Gelation properties of MOP-PEG_{2k} systems

c (Rh-MOP)	n (Rh-MOP) : n (PEG_{2k}-CDI_2)		
	1:3	1:6	1:12
0.7 mM	mucus	mucus	mucus
1.05 mM	mucus	hydrogel	hydrogel
1.4 mM	mucus	hydrogel	hydrogel
2.1 mM	hydrogel	hydrogel	hydrogel
2.8 mM	hydrogel	hydrogel	hydrogel
4.2 mM	hydrogel	hydrogel	hydrogel
5.6 mM	hydrogel	hydrogel	hydrogel

Table S2. Gelation properties of MOP-PEG_{400} systems

c (Rh-MOP)	n (Rh-MOP) : n (PEG_{400}-CDI_2)			
	1:3	1:6	1:12	1:24
0.7 mM	mucus	mucus	mucus	-
1.4 mM	mucus	hydrogel	hydrogel	-
2.1 mM	mucus	hydrogel	hydrogel	-
2.8 mM	mucus	hydrogel	hydrogel	hydrogel
5.6 mM	mucus	hydrogel	hydrogel	hydrogel

Table S3. Gelation properties of MOP-$PEG_{3.4k}$ systems

c (Rh-MOP)	n (Rh-MOP) : n ($PEG_{3.4k}$-CDI_2)			
	1:3	1:6	1:12	1:24
0.7 mM	mucus	mucus	mucus	-
1.4 mM	mucus	mucus	hydrogel	-
2.1 mM	mucus	hydrogel	hydrogel	-
2.8 mM	mucus	hydrogel	hydrogel	hydrogel
5.6 mM	mucus	hydrogel	hydrogel	hydrogel

Table S4. Gelation properties of MOP-PEG_{10k} systems

c (Rh-MOP)	n (Rh-MOP) : n (PEG_{10k}-CDI_2)			
	1:3	1:6	1:12	1:24
0.7 mM	mucus	mucus	mucus	mucus
1.4 mM	mucus	mucus	mucus	mucus
2.8 mM	mucus	mucus	mucus	mucus
5.6 mM	mucus	mucus	mucus	mucus

Table S5. Gelation properties of MOP-4 arms-PEG_{2k} systems

c (Rh-MOP)	n (Rh-MOP) : n (4 arms-PEG_{2k}-CDI)			
	1:3	1:6	1:12	1:24
0.7 mM	mucus	mucus	hydrogel	-
1.4 mM	hydrogel	hydrogel	hydrogel	hydrogel
2.8 mM	hydrogel	hydrogel	hydrogel	hydrogel
5.6 mM	hydrogel	hydrogel	hydrogel	hydrogel

Table S6. Gelation properties of MOP-6 arms-PEG_{2k} systems

c (Rh-MOP)	n (Rh-MOP) : n (6 arms-PEG_{2k}-CDI)				
	1:3	1:6	1:12	1:24	1:48
0.7	hydrogel	hydrogel	hydrogel	hydrogel	-
1.4	hydrogel	hydrogel	hydrogel	hydrogel	-
2.1	hydrogel	hydrogel	hydrogel	hydrogel	-
2.8 mM	hydrogel	hydrogel	hydrogel	hydrogel	precipitation
5.6 mM	hydrogel	hydrogel	hydrogel	hydrogel	precipitation

Table S7. The thermos-behaviors of MOP and telechelic ligands

Samples	N (sites)	KD (M)	Ka (M^{-1})	ΔH (kJ/mol)	ΔG (kJ/mol)	-TΔS (kJ/mol)
PEG_{2k}-Py_2 to Rh-MOP	1.50	15.0e-6	66667	-32.2	-27.6	4.65
PEG_{400}-CDI_2 to Rh-MOP	3.63	102e-6	9804	-47.2	-22.8	24.3
PEG_{2k}-CDI_2 to Rh-MOP	2.60	190e-6	5263	-27.4	-21.3	6.13
$PEG_{3.4k}$-CDI_2 to Rh-MOP	6.21	140e-6	7143	-18.0	-23.5	-5.45
PEG_{10k}-CDI_2 to Rh-MOP	1.38	16.4e-6	60976	-145	-27.3	118
CH_3-PEG_{400}-CDI to Rh-MOP	5.75	140e-6	7143	-18.8	-23.4	-4.57
4 arms-PEG_{2k}-CDI to Rh-MOP	1.34	120e-6	8333	-112.0	-22.4	89.1
6 arms-PEG_{2k}-CDI to Rh-MOP	2.24	34.7e-6	28818	-50.0	-29.6	20.4

Table S8. List of iodine adsorption performances for different adsorbents in water environments

	Materials	Conditions	Iodine adsorption performances ($g\ g^{-1}$)	Ref.
1	SUPE-py-Imine-Cage	1.2 mM iodine solutions, 48 h	8.41	Ref.[7]
2	SUPE-py-Amine-Cage	1.2 mM iodine solutions, 48 h	7.06	Ref.[7]
3	AIMC-1	400 ppm I_2/KI aqueous solution, 8 h	1.03	Ref.[8]
4	C[4]P-DPP	saturated I_2 aqueous solution, 30 min	1.35	Ref.[9]
5	HPOC-101	0.337 mM KI/I_2 aqueous solution, 15 min	1.38	Ref.[10]
6	PyrC	1.2 mM iodine solutions, 6 h	1.81	Ref.[11]
7	HcOF-7	0.12 mM I_2+0.5 mM KI, 6 h at 23 °C	1.39	Ref.[12]
8	H.M.W. resin	100 mg/L I^- solutions, 110 min at 30 °C, pH = 9.0	0.64	Ref.[13]
9	Ag_2O@$Mg(OH)_2$	200 mg/L I^-, 60% within the first 5 min	0.37	Ref.[14]
10	MOP-6 arms PEG_{2k} hydrogels	1 mM iodine solutions, 10.5 min at RT	0.59	This work

5. Reference

1 W. Sun, B. Xue, Q. Fan, R. Tao, C. Wang, X. Wang, Y. Li, M. Qin, W. Wang, B. Chen and Y. Cao, *Sci. Adv.*, *Sci. Adv.*, 2020, **6**, eaaz9531.

2 J. F. Yin, L. Amidani, J. Chen, M. Li, B. Xue, Y. Lai, K. Kvashnina, M. Nyman and P. Yin, *Angew. Chemie - Int. Ed.*, 2024, **63**, e202310953.

3 S. P. O. Danielsen, H. K. Beech, S. Wang, B. M. El-Zaatari, X. Wang, L. Sapir, T. Ouchi, Z. Wang, P. N. Johnson, Y. Hu, D. J. Lundberg, G. Stoychev, S. L. Craig, J. A. Johnson, J. A. Kalow, B. D. Olsen and M. Rubinstein, *Chem. Rev.*, 2021, **121**, 5042–5092.

4 A. Carné-Sánchez, J. Albalad, T. Grancha, I. Imaz, J. Juanhuix, P. Larpent, S. Furukawa and D. Maspoch, *J. Am. Chem. Soc.*, 2019, **141**, 4094–4102.

5 H. Xiao, J. F. Yin, Q. Cheng, Q. Zhou, J. Chen, C. Huang and P. Yin, *ACS Appl. Nano Mater.*, 2021, **4**, 10430–10437.

6 T. Grancha, A. Carné-Sánchez, L. Hernández-López, J. Albalad, I. Imaz, J. Juanhuix and D. Maspoch, *J. Am. Chem. Soc.*, 2019, **141**, 18349–18355.

7 W. Zhou, A. Li, M. Zhou, Y. Xu, Y. Zhang and Q. He, *Nat. Commun.*, 2023, **14**, 25–31.

8 Y. J. Liu, Y. F. Sun, S. H. Shen, S. T. Wang, Z. H. Liu, W. H. Fang, D. S. Wright and J. Zhang, *Nat. Commun.*, 2022, **13**, 1–10.

9 L. Xie, Z. Zheng, Q. Lin, H. Zhou, X. Ji, J. L. Sessler and H. Wang, *Angew. Chemie - Int. Ed.*, 2022, **61**, e202113724.

10 M. Yang, F. Qiu, E. S. M. El-Sayed, W. Wang, S. Du, K. Su and D. Yuan, *Chem. Sci.*, 2021, **12**, 13307–13315.

11 Z. Y. Zeng, Z. C. Lou, L. Hu, W. Dou, X. Zhao, X. Li, J. Fang, X. Qian, H. B. Yang and L. Xu, *Chem. Eng. J.*, 2024, **496**, 154091.

12 M. Zhang, J. Samanta, B. A. Atterberry, R. Staples, A. J. Rossini and C. Ke, *Angew. Chemie*, 2022, **134**, e202214189.

13 W. Mu, Q. Yu, X. Li, H. Wei and Y. Jian, *RSC Adv.*, 2016, **6**, 81719–81725.

14 Y. Y. Chen, S. H. Yu, Q. Z. Yao, S. Q. Fu and G. T. Zhou, *J. Colloid Interface Sci.*, 2018, **510**, 280–291.